Chiral phase transition in soft-wall AdS/QCD with scalar-dilaton coupling

Sean P. Bartz[*], Robert C. Meadows, and Glenn Brock

Department of Chemistry and Physics, Indiana State University, Terre Haute, Indiana 47809, USA

The chiral phase boundary of nuclear matter is expected to have a critical point where the rapid crossover of lattice methods at zero chemical potential becomes a first-order phase transition. Phenomenological models based on the AdS/CFT correspondence, known as AdS/QCD, have succeeded in capturing many features of nuclear matter, with recent progress in producing the expected critical point. We study a model that produces a critical point in the chiral phase diagram by introducing a coupling between the scalar chiral field and the dilaton. We examine the effect of the scalar-dilaton coupling on the critical point. We also study the zero-temperature chiral dynamics, which must allow for spontaneous chiral symmetry breaking in the limit of zero quark mass. We find that when the scalar-dilaton coupling is large enough to ensure correct zero-temperature chiral dynamics, a critical point is present only if the quark mass is greater than 12.8 MeV.

I. INTRODUCTION

The exploration of the phase structure of quantum chromodynamics (QCD) at extreme temperature and density is an important project for both theory and experiment [1–3]. Lattice QCD finds a crossover phase transition at zero quark chemical potential [4,5], while other models find a first-order phase transition at high chemical potential [6]. In combination, these models suggest the existence of a critical point, but its exact location in the phase diagram remains an open question [7,8].

Experimentally, the search for the critical point requires a reduction in center of mass energy [9], motivating the recently completed beam energy scan at the Relativistic Heavy Ion Collider [10], as well as current and future fixed-target experiments [11–13]. From the theoretical perspective, lattice methods suffer from a well-known sign problem at finite chemical potential [14]. Extrapolation techniques allow lattice analysis up to a baryon chemical potential ≈ 300 MeV, with no evidence of a critical point [15].

The AdS/CFT correspondence [16–18] has emerged as a powerful tool to study various aspects of QCD, including the phase diagram [19,20]. The soft-wall AdS/QCD model, which uses a background dilaton field to encode confinement, has been extensively used to analyze hadron spectra [21,22] and the QCD phase diagram [23]. While there has been success in finding a critical point in the deconfinement phase transition using holographic techniques [24–32], producing a critical point in the chiral phase transition has been more elusive.

In this work, we consider a modified soft-wall AdS/QCD model with a coupling between the scalar and dilaton fields. Prior work has shown that the introduction of such a coupling can improve the resulting meson spectra and introduce a critical point in the chiral phase diagram [33]. We focus on the effect of scalar-dilaton coupling on the critical point in the QCD phase diagram and the zero-temperature chiral dynamics.

II. SOFT-WALL MODEL WITH SCALAR-DILATON COUPLING

We use an anti–de Sitter (AdS) black hole metric

$$ds^2 = \frac{L^2}{z^2}\left(-f(z)dt^2 + dx_i^2 + \frac{dz^2}{f(z)}\right), \qquad (1)$$

with the AdS curvature $L = 1$ throughout the rest of this work. Following established procedure [34–36], we model finite temperature and chemical potential with a charged black hole described by the 5D AdS-Reissner-Nordström blackness function

$$f(z) = 1 - (1 + Q^2)\left(\frac{z}{z_h}\right)^4 + Q^2\left(\frac{z}{z_h}\right)^6, \qquad (2)$$

where z_h is the black hole horizon, and Q is related to the black hole charge q by $Q = qz_h^3$. The quark chemical potential and temperature are determined by the charge and horizon position

[*]Contact author: sean.bartz@indstate.edu

$$\mu = \kappa \frac{Q}{z_h}, \tag{3}$$

$$T = \frac{1}{\pi z_h}\left(1 - \frac{Q^2}{2}\right), \tag{4}$$

where $0 < Q^2 < 2$ and $\kappa = 1$ [37]. Note that μ is the quark chemical potential, with a value one-third of the baryon chemical potential. These relationships are invertible for z_h and q.

In the soft-wall model of AdS/QCD, confinement is introduced via a dilaton field that smoothly cuts off the action, as opposed to a hard cutoff of the holographic coordinate [21]. The dilaton is required to be quadratic in the IR limit to produce linear confinement as evidenced by radially excited meson spectra $m_n^2 \sim n$ [22]. Previous work has considered UV modifications to the dilaton to achieve proper chiral dynamics [38–41], but this is not necessary in a model with chiral-dilaton coupling [42]. For simplicity, we use a purely quadratic dilaton

$$\Phi(z) = \mu_g^2 z^2 \tag{5}$$

where $\mu_g \sim \Lambda_{\text{QCD}}$ sets the confinement scale. Following [43], which determined the parameters by a global fit to meson spectra, we take $\mu_g = 440$ MeV.

The relevant matter fields are described by the action

$$S = \frac{1}{2k}\int d^5x \sqrt{-g}\, e^{-\Phi(z)}\big\{\text{Tr}[|DX|^2 + V_m(X, \Phi)]$$
$$+ \gamma \text{Re}[\det(X)]\big\}, \tag{6}$$

where X contains the scalar and pseudoscalar meson fields. The 't Hooft determinant term provides mixing between light and heavy flavors. We omit the vector and axial-vector meson fields to focus on the chiral dynamics.

A quartic term in the scalar potential is required for spontaneous chiral symmetry breaking [38]. Including the coupling between the dilaton and scalar field, the potential is

$$V_m(X, \Phi) = m_5^2|X|^2 + \lambda_1\Phi|X|^2 + 4\lambda_4|X|^4. \tag{7}$$

The AdS/CFT dictionary sets the 5D masses of the fields $m_5^2 = (\Delta - p)(\Delta + p - 4)$, where Δ is the dimension of the corresponding p-form QCD operator [18,21]. The scalar field is dual to the $\bar{q}q$ operator, so its mass is $m_5^2 = -3$. In this flavor-symmetric model, we are most interested in qualitative behavior, which is not very sensitive to the values of the free parameters in the scalar potential, as long as the 't Hooft determinant coefficient γ is negative to produce a first-order transition in the chiral limit [39]. For the sake of comparison, we choose values equivalent to the model in [44], setting $\lambda_4 = 4.2$ and $\gamma = -22.6$, with the fitting of
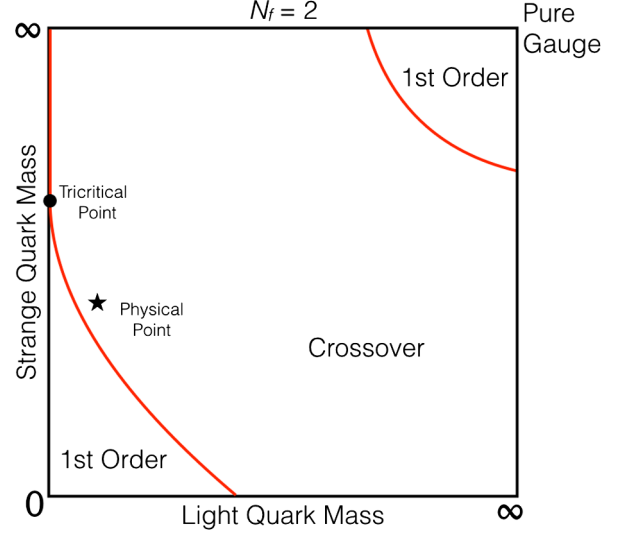

FIG. 1. A sketch of the Columbia plot, which shows the expected order of the chiral phase transition as a function of light and strange quark masses [46,47].

these values to experimental data reserved for an anticipated $2 + 1$-flavor version of this model.

The scalar-dilaton coupling term gives the chiral field an effective mass that runs with energy scale

$$m_5^2 \to -3 + \lambda_1\mu_g^2 z^2. \tag{8}$$

This running mass has been used to obtain the correct mass splitting between excited states of meson chiral partners [43], to reproduce the Columbia plot (Fig. 1) at zero chemical potential [44], to obtain the correct chiral transition behavior [42], and to produce a critical point in the chiral phase diagram [33]. It is worth noting that models with a modified dilaton profile but without the running mass (8) achieve the first three of these goals [39,40] but do not produce the critical point [45].

The scalar field has a z-dependent vacuum expectation value (VEV) that describes the chiral symmetry breaking of the model. In a three-flavor model, the VEV becomes

$$\langle X \rangle = \frac{1}{\sqrt{2}}\begin{pmatrix} \chi_u(z) & 0 & 0 \\ 0 & \chi_d(z) & 0 \\ 0 & 0 & \chi_s(z) \end{pmatrix}. \tag{9}$$

In this work, we will focus on the flavor-symmetric case $\chi_u = \chi_d = \chi_s$. Varying (6) with respect to χ yields the following equation of motion:

$$\chi'' - \left(\frac{3}{z} + \Phi' - \frac{f'}{f}\right)\chi'$$
$$- \frac{1}{z^2 f}\big[(-3 - \lambda_1\Phi)\chi + 4\lambda_4\chi^3 + 3\lambda_3\chi^2\big] = 0, \tag{10}$$

where $\gamma \to 6\sqrt{2}\lambda_3$ is defined for convenient notation. As the chiral field is the source of the $\bar{q}q$ operator, the AdS/CFT dictionary identifies its coefficients at the UV boundary with the sources of chiral symmetry breaking,

$$\chi(z \to 0) \sim m_q \zeta z + \frac{\sigma}{\zeta} z^3, \tag{11}$$

where $\zeta = \sqrt{N_c}/(2\pi)$ [48], the quark mass m_q is the source of explicit chiral symmetry breaking, and the chiral condensate σ is the source of spontaneous chiral symmetry breaking.

III. NUMERICAL PROCEDURE

Finding the chiral condensate requires solving (10) numerically and using the AdS/CFT dictionary to relate the solution for $\chi(z)$ to the parameters m_q, σ. The presence of a singular point at $z = z_h$ presents a challenge to this procedure. A commonly used numerical method begins with a UV approximation for the chiral field and integrates toward the horizon [40,43,49]. While this method works well near the chiral transition temperature, it is less reliable at low temperatures. Instead, we use a method that starts with the asymptotic solution at the black hole horizon z_h and integrates toward the UV boundary [41]. A comparison between these two methods is discussed in the Appendix.

The near-horizon solution is approximated by the Taylor series

$$\chi(u \to 1) = d_0 + d_1(1 - u) + d_2(1 - u)^2 + \dots \tag{12}$$

where $u = z/z_h$ and the higher-order coefficients are solved by substitution into (10). The result is

$$d_1 = \frac{d_0}{2(Q^2 - 2)} \left(3 + \lambda_1 z_h^2 \mu_g^2 - 3d_0\lambda_3 - 4d_0^2\lambda_4\right), \tag{13}$$

$$d_2 = \frac{1}{16(Q^2 - 2)^2} \Big\{ 6d_1(-6 + Q^2 + Q^4) + 4d_0^3(14 - 13Q^2)\lambda_4$$
$$+ d_0^2 \big[(42 - 39Q^2)\lambda_3 - 24d_1(Q^2 - 2)\lambda_4\big] - 2d_1(Q^2 - 2)(4Q^2 - 8 - \lambda_1)z_h^2\mu_g^2$$
$$+ 3d_0\big[-14 + 13Q^2 + 8d_1\lambda_3 - 4d_1Q^2\lambda_3 + \lambda_1(3Q^2 - 2)z_h^2\mu_g^2\big] \Big\}. \tag{14}$$

For each value of T, μ, we vary d_0 and compare the numerical solution to the UV expansion of the chiral field

$$\chi(u \to 0) \approx m_q \zeta z_h u - 3m_q^2 \zeta^2 \lambda_3 z_h^2 u^2 + \frac{\sigma}{\zeta} z_h^3 u^3 + \frac{1}{4}\big[m_q^3 \zeta^3(\lambda_4 - 36\lambda_3^2) + 2m_q \zeta\mu_g^2(\lambda_1 - 2)\big]z_h^3 u^3 \log(z_h u) + \dots . \tag{15}$$

The terms of order u and u^3 have their coefficients defined by the AdS/CFT dictionary and the other coefficients are found by solving (10) order by order.

We evaluate the numerical solution and its derivative at a small value $u_i \approx 10^{-3}$ and calculate the coefficients by comparing to the UV expansion (15). Keeping terms up to order u^3, the relationships are analytically solvable,

$$m_q = \frac{1 - \sqrt{1 - 3\lambda_3(3\chi_{\mathrm{UV}} - u_i\chi'_{\mathrm{UV}})}}{3\lambda_3 \zeta u_i z_h}, \tag{16}$$

$$\sigma = \zeta \left(\frac{1 - 3\lambda_3(2\chi_{\mathrm{UV}} + u_i\chi'_{\mathrm{UV}}) - \sqrt{1 - 3\lambda_3(3\chi_{\mathrm{UV}} - u_i\chi'_{\mathrm{UV}})}}{3u_i^3 z_h^3 \lambda_3} \right), \tag{17}$$

where $\chi_{\mathrm{UV}} = \chi(u_i)$ and $\chi'_{\mathrm{UV}} = \chi'(u_i)$. The quadratic relationship has another set of solutions, which produce unphysical values of $m_q, \sigma < 0$. In the two-flavor case, $\lambda_3 = 0$ and the above relationships cannot be used. Instead we find

$$m_q = \frac{3\chi_{\mathrm{UV}} - u_i\chi'_{\mathrm{UV}}}{2\zeta z_h u_i}, \tag{18}$$

$$\sigma = \zeta \frac{u_i\chi'_{\mathrm{UV}} - \chi_{\mathrm{UV}}}{2z_h^3 u_i^3}. \tag{19}$$

IV. RESULTS

In this section, we find the dependence of the chiral condensate σ on quark mass m_q for various values of the scalar-dilaton coupling λ_1. We show that there is a minimum value of λ_1 that allows for spontaneous chiral symmetry breaking in the chiral limit $m_q \rightarrow 0$. We show how the (pseudo)critical temperature is found and how crossover and first-order transitions are distinguished. Finally, we show how the location of the critical point is affected by the value of λ_1.

A. Spontaneous chiral symmetry breaking

Separate sources of spontaneous and explicit chiral symmetry breaking are required in the theory. The original soft-wall model did not achieve this, finding $\sigma \sim m_q$ instead [22]. Including a quartic term in the scalar potential allows these quantities to be independent, crucially maintaining spontaneous chiral symmetry breaking in the chiral limit $m_q = 0$ [38].

The relationship between m_q and σ in this model depends on the strength of the scalar-dilaton coupling λ_1. We check this relationship in both the two-flavor ($\lambda_3 = 0$) and three-flavor ($\lambda_3 \neq 0$) cases. In the two-flavor case, the relationship between σ and m_q is one-to-one for quark mass $m_q \geq 0$. For small values of the scalar-dilaton coupling, the spontaneous chiral symmetry breaking vanishes as $m_q \rightarrow 0$, but at higher values of $\lambda_1 \geq 6.0$, σ is nonzero in the chiral limit, as seen in Fig. 2.

In the three-flavor case, we find the same requirement $\lambda_1 \geq 6.0$ for σ to remain finite as the quark mass goes to zero. In Fig. 3, it is evident that σ becomes multivalued for intermediate values of λ_1. In these cases, the smaller value of σ is thermodynamically favored. This means that in the
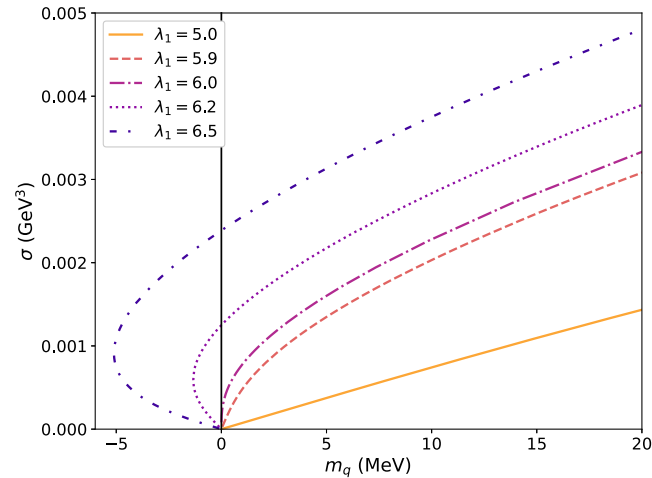

FIG. 2. The relationship between σ and m_q for a variety of values of the scalar-dilaton coupling λ_1 with two flavors at zero temperature and chemical potential. For $\lambda_1 \geq 6.0$, the chiral condensate is present even in the chiral limit $m_q = 0$.
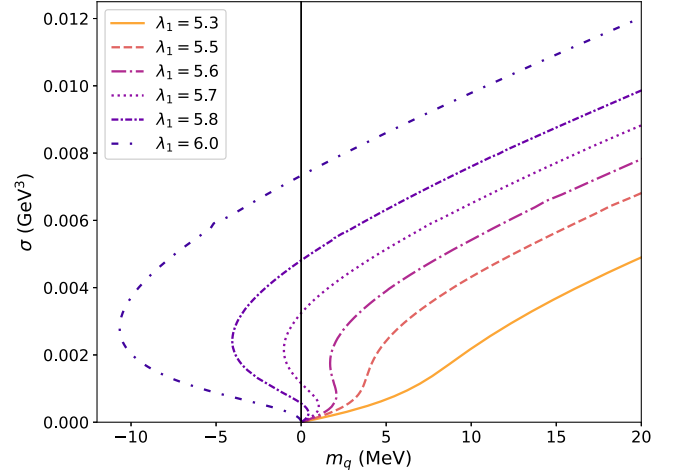

FIG. 3. The relationship between σ and m_q for a variety of values of the scalar-dilaton coupling λ_1 with three flavors. When σ is multivalued, the lowest value is thermodynamically favored. For $\lambda_1 \geq 6.0$, the chiral condensate is present even in the chiral limit $m_q = 0$.

case of e.g., $\lambda_1 = 5.7$ it appears that there are finite solutions of σ at zero quark mass, but these solutions are unphysical, and the lower branch of the graph shows $\sigma \sim m_q$ at small quark mass for these values of λ_1.

Another hallmark of chiral symmetry breaking is the Gell-Mann–Oakes–Renner (GOR) relation, which relates the pion mass and pion decay constant to the quark mass and chiral condensate, $2m_q\sigma = f_\pi^2 m_\pi^2$ [50]. The GOR relation arises from the minimal AdS/QCD setup, through an analysis of the axial-vector and pseudoscalar sectors [21,22,51]. The equations of motion for these sectors are not directly coupled to the scalar potential, so considering higher-order terms in the scalar potential does not affect this result, which has been confirmed numerically [41,43,52]. Numerical investigation of meson spectra and the GOR relation is reserved for future work.

B. Chiral phase transition

For a given value of the chemical potential μ and quark mass m_q, we find the values of σ for a range of temperatures. The order of the chiral phase transition is determined by the way in which σ transitions to a smaller value. Smooth transitions are considered crossover, while a first-order phase transition is characterized by the chiral condensate becoming multivalued, as illustrated in Fig. 4.

In crossover transitions, the pseudocritical temperature is the temperature where the chiral susceptibility $|d\sigma/dT|$ is maximized. For first-order transitions, the critical temperature occurs at the lowest temperature where σ is multivalued.

The values of λ_1 that produce unphysical chiral dynamics at zero temperature also show unphysical behavior in the chiral phase transition. The chiral condensate is plotted as a
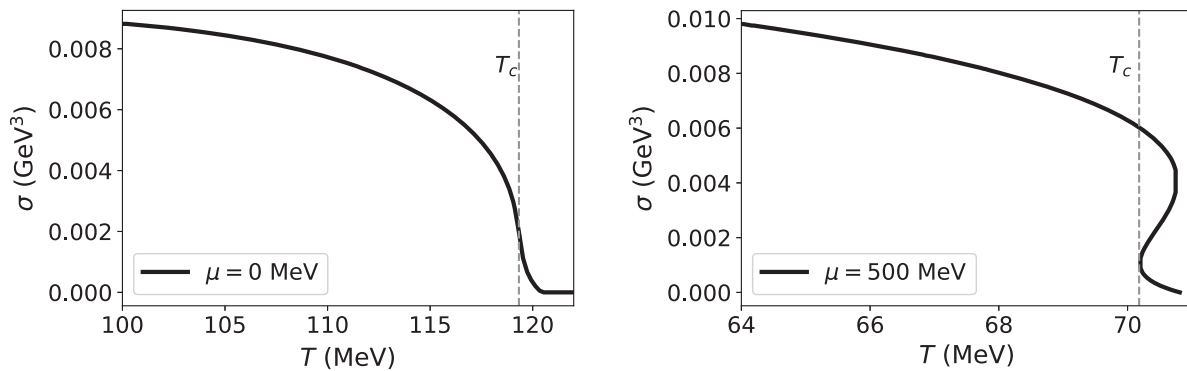
FIG. 4. These plots illustrate the difference between a crossover phase transition and a first-order phase transition. At zero chemical potential (left), the transition is smooth, but at higher μ (right), the value of σ becomes multivalued, indicating a first-order phase transition. Both plots use $m_q = 15$ MeV and $\lambda_1 = 6$.
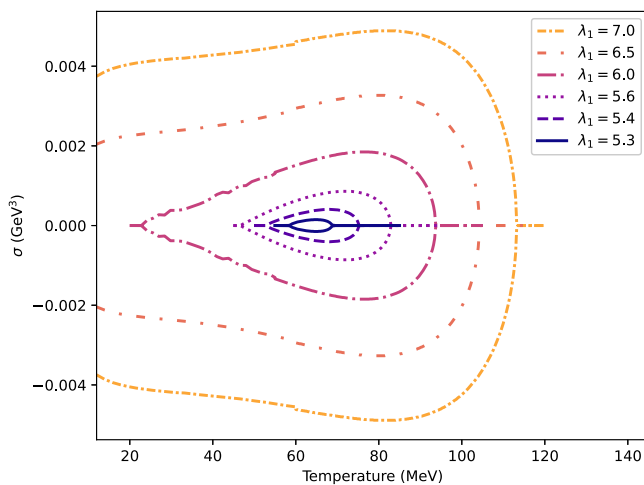

FIG. 5. The two-flavor results in the chiral limit for chiral condensate σ as a function of temperature at zero chemical potential. For scalar-dilaton coupling $\lambda_1 \leq 6$, σ vanishes at low temperatures.
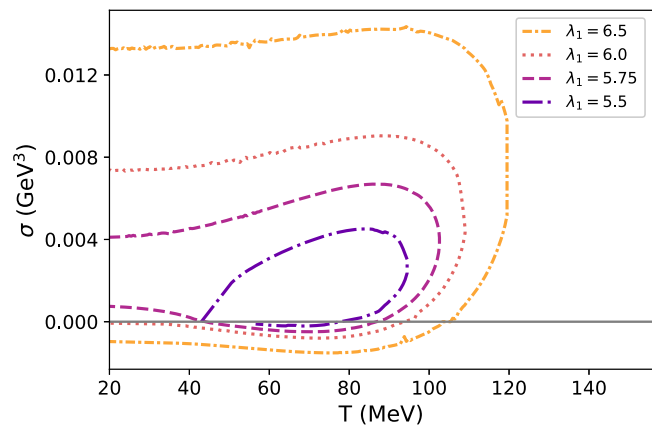

FIG. 6. The three-flavor results in the chiral limit for chiral condensate σ as a function of temperature at zero chemical potential. For scalar-dilaton coupling $\lambda_1 \leq 5.5$, σ vanishes at low temperatures.

function of temperature at $\mu = 0$ in the chiral limit for two flavors (Fig. 5) and three flavors (Fig. 6). Note that the two-flavor case allows negative values of $\sigma \leftrightarrow -\sigma$ as solutions. This symmetry is broken in the three-flavor case and also when $m_q > 0$, although negative solutions are still present [39]. These nonphysical solutions are ignored in the rest of the analysis.

The chiral phase transition has the expected low T behavior in the chiral limit. As this parameter is decreased, the "bump" below the critical temperature becomes more pronounced. When λ_1 is below a certain value, the chiral condensate disappears at low temperature. This unphysical result is further evidence for a minimum value for the scalar-dilaton coupling in this model.

C. Phase diagram and critical point

The chiral phase diagram is produced by plotting the (pseudo)critical temperature as a function of the chemical potential. A critical end point is found for combinations of m_q and λ_1 that produce a crossover phase transition at zero chemical potential. At sufficiently large μ, the phase transition becomes first order.

To examine the effect of scalar-dilaton coupling on the location of the critical point, we show in Fig. 7 phase boundaries for a sample quark mass $m_q = 15$ for varying λ_1 with three symmetric quark flavors. The critical point occurs at smaller chemical potential as λ_1 is increased. At the same time, the (pseudo)critical temperature is increased at all values of μ.

When the scalar-dilaton coupling is sufficiently large, the phase transition is first order at $\mu = 0$, and the critical point vanishes. This is seen in Fig. 8, where the location of the critical point is plotted for several values of the quark mass. When the quark mass is large, a critical point can still be found when $\lambda_1 \geq 6.0$, as required for the proper chiral dynamics detailed in Sec. IV A. At low values of the quark mass, obtaining a critical point requires $\lambda_1 < 6.0$. We find that the minimum quark mass with a critical point in the
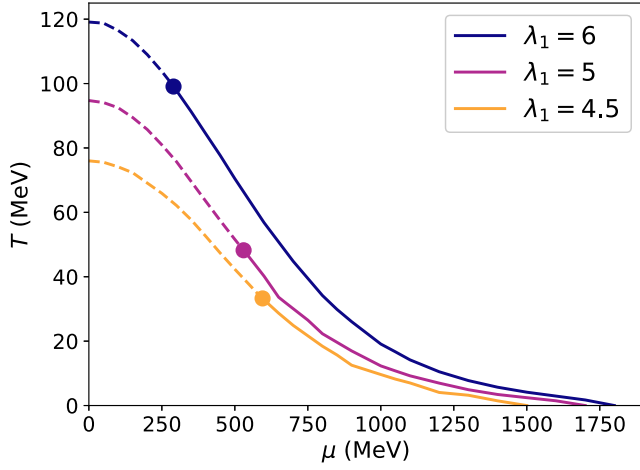
FIG. 7. The phase diagram is shown for $m_q = 15$ MeV for various values of the scalar-dilaton coupling parameter λ_1. Dashed lines indicate a crossover and solid lines indicate a first-order phase transition. The critical points are indicated by a large dot. Increasing λ_1 moves the critical point to smaller chemical potential values while also increasing the crossover temperature at $\mu = 0$.
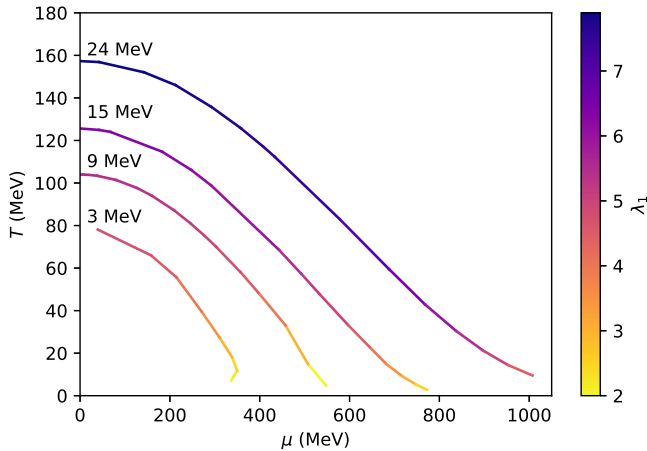

FIG. 8. The locations of the critical point for different values of the quark mass and scalar-dilaton coupling λ_1 are shown. The curves are labeled by the value of the quark mass.

phase diagram when $\lambda_1 = 6.0$ is $m_q = 12.8$ MeV. In the chiral limit, we find that the chiral phase transition is always first order, regardless of the value of λ_1, and no critical point is present.

V. DISCUSSION

In this work, we used a soft-wall holographic QCD model with a scalar-dilaton coupling to study the chiral phase transition at finite temperature and density. Our analysis shows that a coupling $\lambda_1 \geq 6.0$ is necessary for achieving the correct chiral dynamics with either two or three symmetric quark flavors, in line with the requirement that holographic models mirror the chiral symmetry breaking mechanism of QCD [21,22]. Furthermore, the presence of a critical point in this model's chiral phase diagram contributes to the ongoing effort to comprehend the phase structure of QCD, a topic of considerable theoretical and experimental interest [53,54].

Previous soft-wall AdS/QCD models that achieved correct chiral dynamics at zero chemical potential by using a UV-modified dilaton [39,45] could be extended to include a scalar-dilaton coupling term. It may be interesting to examine whether this will circumvent the problems shown in the current work at small values of the scalar-dilaton coupling.

Looking ahead, we will allow the strange quark mass to differ from the light quark masses and explore the $2+1$-flavor results at a range of scalar-dilaton coupling. These results will be compared to the Columbia plot shown in Fig. 1. Another goal is to combine the analysis of the chiral transition with the deconfinement phase transition. Previous work combining a scalar chiral field with the dynamical Einstein-Maxwell-dilaton model have shown some promise in the case of two quark flavors [55]. Including the scalar-dilaton mixing term produces the crossover chiral transition that is expected for two quark flavors with $m_q > 0$ [56]. Considering these extensions will allow a more thorough exploration of all aspects of the holographic QCD phase diagram.

APPENDIX: COMPARISON OF NUMERICAL METHODS

Another commonly used numerical method for solving the chiral equation of motion (10) uses the UV expansion of (15) as one boundary condition and the regularity of the chiral field at the horizon $z = z_h$ is used as the other. Regularity is difficult to check numerically, so a "test" function is defined that includes all the potentially singular parts of the equation of motion,

$$-z^2 \frac{f'(z)}{f(z)} \chi'(z) + \frac{1}{f(z)} \left[(-3 - \lambda_1 \Phi)\chi + 4\lambda_4 \chi^3 + 3\lambda_3 \chi^2 \right].$$

(A1)

This collection of terms must be zero at the horizon, otherwise there will be a divergence as $f \to 0$. Ensuring
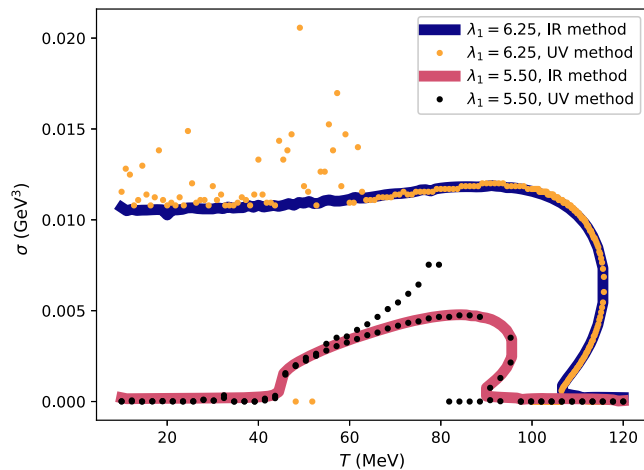
FIG. 9. This comparison of the numerical methods shows agreement between them, but more spurious points when integrating from the UV. The data shown are for two representative values of the scalar-dilaton coupling λ_1 with $m_q = 1$ MeV and $\mu = 0$.

the test function is zero becomes the second boundary condition.

The shooting method [57] is implemented with the required quark mass given as an input parameter and σ varied until the boundary condition is met near the black hole horizon. This method is used to find the allowed values of σ for a given T, μ, and m_q.

The limitations of this method are revealed at low temperature $T \ll T_c$. At low temperature, $z_h \sim T^{-1}$ becomes large, and numerical instabilities in the numerical solution to (10) make it difficult to determine the correct value of σ. This has not been a problem in previous publications that focus on the chiral phase transition. Typically, the value of σ approaches a constant value as temperature is decreased below the transition temperature. However, this is not always the case in this model, where $\sigma = 0$ at low temperatures for some values of λ_1, as seen in Fig. 9.

The method of integrating from the UV boundary is trustworthy near the transition temperature. However, in this work we are also interested in the low temperature chiral dynamics, particularly in ensuring separate sources of explicit and spontaneous chiral symmetry breaking, as discussed in Sec. IV A. By starting near the singular point and integrating away from it, the method of Sec. III is more numerically stable at lower temperatures.

[1] H. Elfner and B. Müller, J. Phys. G **50**, 103001 (2023).
[2] X. An *et al.*, Nucl. Phys. **A1017**, 122343 (2022).
[3] A. Pandav, D. Mallick, and B. Mohanty, Prog. Part. Nucl. Phys. **125**, 103960 (2022).
[4] Y. Aoki, G. Endrődi, Z. Fodor, S. D. Katz, and K. K. Szabó, Nature (London) **443**, 675 (2006).
[5] G. Aarts *et al.*, Prog. Part. Nucl. Phys. **133**, 104070 (2023).
[6] K. Fukushima and C. Sasaki, Prog. Part. Nucl. Phys. **72**, 99 (2013).
[7] R. Bellwied, S. Borsányi, Z. Fodor, J. Günther, S. Katz, A. Pásztor, C. Ratti, and K. Szabó, Nucl. Phys. **A956**, 797 (2016).
[8] P. J. Gunkel and C. S. Fischer, Phys. Rev. D **104**, 054022 (2021).
[9] L. Adamczyk *et al.*, Phys. Rev. Lett. **112**, 032302 (2014).
[10] STAR Collaboration, arXiv:1007.2613.
[11] K. Meehan, Nucl. Phys. **A967**, 808 (2017).
[12] T. Ablyazimov *et al.*, Eur. Phys. J. A **53**, 60 (2017).
[13] D. Almaalol *et al.*, arXiv:2209.05009.
[14] O. Philipsen, Prog. Part. Nucl. Phys. **70**, 55 (2013).
[15] S. Borsanyi, Z. Fodor, J. N. Guenther, R. Kara, S. D. Katz, P. Parotto, A. Pasztor, C. Ratti, and K. K. Szabó, Phys. Rev. Lett. **125**, 052001 (2020).
[16] J. Maldacena, Adv. Theor. Math. Phys. **2**, 231 (1998).
[17] E. Witten, Adv. Theor. Math. Phys. **2**, 505 (1998).
[18] E. Witten, Adv. Theor. Math. Phys. **2**, 253 (1998).
[19] S. S. Gubser and A. Nellore, Phys. Rev. D **78**, 086007 (2008).
[20] S. S. Gubser, A. Nellore, S. S. Pufu, and F. D. Rocha, Phys. Rev. Lett. **101**, 131601 (2008).
[21] J. Erlich, E. Katz, D. T. Son, and M. A. Stephanov, Phys. Rev. Lett. **95**, 261602 (2005).
[22] A. Karch, E. Katz, D. T. Son, and M. A. Stephanov, Phys. Rev. D **74**, 015005 (2006).
[23] R. Rougemont, J. Grefa, M. Hippert, J. Noronha, J. Noronha-Hostler, I. Portillo, and C. Ratti, Prog. Part. Nucl. Phys. **135**, 104093 (2024).
[24] O. DeWolfe, S. S. Gubser, and C. Rosen, Phys. Rev. D **83**, 086005 (2011).
[25] O. DeWolfe, S. S. Gubser, and C. Rosen, Phys. Rev. D **84**, 126014 (2011).
[26] Z. Li, Y. Chen, D. Li, and M. Huang, Chin. Phys. C **42**, 013103 (2018).
[27] R. Critelli, J. Noronha, J. Noronha-Hostler, I. Portillo, C. Ratti, and R. Rougemont, Phys. Rev. D **96**, 096026 (2017).
[28] R. Rougemont, R. Critelli, and J. Noronha, Phys. Rev. D **98**, 034028 (2018).
[29] J. Grefa, J. Noronha, J. Noronha-Hostler, I. Portillo, C. Ratti, and R. Rougemont, Phys. Rev. D **104**, 034002 (2021).
[30] R.-G. Cai, S. He, L. Li, and Y.-X. Wang, Phys. Rev. D **106**, L121902 (2022).
[31] M. Hippert, J. Grefa, T. A. Manning, J. Noronha, J. Noronha-Hostler, I. P. Vazquez, C. Ratti, R. Rougemont, and M. Trujillo, arXiv:2309.00579.
[32] Q. Fu, S. He, L. Li, and Z. Li, arXiv:2404.12109.

[33] Z. Fang, Y.-L. Wu, and L. Zhang, Phys. Rev. D **99**, 034028 (2019).

[34] A. Chamblin, R. Emparan, C. V. Johnson, and R. C. Myers, Phys. Rev. D **60**, 064018 (1999).

[35] C. Park, Phys. Rev. D **81**, 045009 (2010).

[36] P. Colangelo, F. Giannuzzi, and S. Nicotri, Phys. Rev. D **83**, 035015 (2011).

[37] P. Colangelo, F. Giannuzzi, S. Nicotri, and V. Tangorra, Eur. Phys. J. C **72**, 2096 (2012).

[38] T. Gherghetta, J. I. Kapusta, and T. M. Kelley, Phys. Rev. D **79**, 076003 (2009).

[39] K. Chelabi, Z. Fang, M. Huang, D. Li, and Y.-L. Wu, J. High Energy Phys. 04 (2016) 036.

[40] S. P. Bartz and T. Jacobson, Phys. Rev. D **94**, 075022 (2016).

[41] A. Ballon-Bayona, L. A. H. Mamani, and D. M. Rodrigues, Phys. Rev. D **104**, 126029 (2021).

[42] Z. Fang and Y.-L. Wu, Chin. Phys. C **44**, 103101 (2020).

[43] Z. Fang, Y.-L. Wu, and L. Zhang, Phys. Lett. B **762**, 86 (2016).

[44] Z. Fang, Y.-L. Wu, and L. Zhang, Phys. Rev. D **98**, 114003 (2018).

[45] S. P. Bartz and T. Jacobson, Phys. Rev. C **97**, 044908 (2018).

[46] F. R. Brown, F. P. Butler, H. Chen, N. H. Christ, Z. Dong, W. Schaffer, L. I. Unger, and A. Vaccarino, Phys. Rev. Lett. **65**, 2491 (1990).

[47] P. de Forcrand and O. Philipsen, J. High Energy Phys. 01 (2007) 077.

[48] A. Cherman, T. D. Cohen, and E. S. Werbos, Phys. Rev. C **79**, 045203 (2009).

[49] D. Li, M. Huang, and Q.-S. Yan, Eur. Phys. J. C **73**, 2615 (2013).

[50] M. Gell-Mann, R. J. Oakes, and B. Renner, Phys. Rev. **175**, 2195 (1968).

[51] A. Cherman, T. D. Cohen, and E. S. Werbos, Phys. Rev. C **79**, 045203 (2009).

[52] T. M. Kelley, S. P. Bartz, and J. I. Kapusta, Phys. Rev. D **83**, 016002 (2011).

[53] K. Rajagopal, Nucl. Phys. **A661**, 150 (1999).

[54] E. Laermann and O. Philipsen, Annu. Rev. Nucl. Part. Sci. **53**, 163 (2003).

[55] Y. Yang and P.-H. Yuan, Phys. Lett. B **832**, 137212 (2022).

[56] X.-Y. Liu, X.-C. Peng, Y.-L. Wu, and Z. Fang, Phys. Rev. D **109**, 054032 (2024).

[57] W. H. Press, S. A. Teukolsky, W. T. Vetterling, and B. P. Flannery, *Numerical Recipes 3rd Edition: The Art of Scientific Computing*, 3 ed. (Cambridge University Press, Cambridge, England, 2007).